

# Magnetic properties of a mixed spin-1/2 and spin-3/2 Ising model with an uniaxial and biaxial crystal-field potential<sup>1</sup>

Michal Jaščur and Jozef Strečka<sup>\*</sup>

*Department of Theoretical Physics and Astrophysics, Faculty of Science,  
P. J. Šafárik University, Park Angelinum 9, 041 54 Košice, Slovak Republic*

---

## Abstract

Magnetic properties of a mixed spin-1/2 and spin-3/2 Ising model on honeycomb lattice are investigated within the framework of an exact star-triangle mapping transformation. The particular attention is focused on the effect of uniaxial and biaxial crystal-field potentials that basically influence the magnetic behaviour of the spin-3/2 atoms. Our results for the basic thermodynamic quantities, as well as the dynamical time-dependent autocorrelation function indicate the spin tunneling between the  $|\pm \frac{3}{2}\rangle$  and  $|\mp \frac{1}{2}\rangle$  states in two different magnetically ordered phases OP<sub>1</sub> and OP<sub>2</sub>, respectively.

*Key words:* uniaxial and biaxial crystal-field potential, star-triangle transformation, spin dynamics, exact solution

*PACS:* 75.10.Hk, 05.50.+q

---

## 1 Introduction

During the last decade, a quantum tunneling of magnetization has become among the most actively studied topics in the condensed matter physics. The immense interest aimed at better understanding of this quantum phenomenon has been mainly stimulated by a recent experimental observation of the quantum spin tunneling in a large number of single-molecule magnets (see Ref.

---

<sup>\*</sup> Corresponding author.

*Email addresses:* jascur@upjs.sk (Michal Jaščur), jozkos@pobox.sk (Jozef Strečka).

<sup>1</sup> This work was financially supported by the VEGA grant No. 1/9034/02 and the APVT grant No. 20-009902.

[1] and references therein). By the term single-molecule magnet one denotes an assembly of weakly interacting clusters of magnetic metal atoms that usually possess an extraordinary strong magnetic anisotropy. Hence, the single-molecule magnets often provide very good examples of magnetic systems with a strong uniaxial magnetocrystalline anisotropy, i. e. so-called Ising-like spin systems. Of course, the Ising anisotropy by itself cannot be a source of the quantum spin tunneling experimentally observed in these systems. It turns out, however, that this quantum phenomenon arises in the most cases due to the higher-order crystal-field terms. According to a number of experimental and theoretical studies it is now quite well established that the spin tunneling observed in  $\text{Fe}_4$  [2],  $\text{Fe}_8$  [3],  $\text{Fe}_{19}$  [4], or  $\text{Mn}_4$  [5] compounds originates to a major extent from the second-order biaxial crystal-field potential.

With regard to this, the extensive studies focused on the magnetic properties of small clusters shed light on the effect of single-ion anisotropy terms  $D$  (uniaxial anisotropy) and  $E$  (biaxial, also called rhombic anisotropy). In contrast to the quite well understood role of both the single-ion anisotropies in the small magnetic clusters (zero-dimensional systems), the situation becomes much more complex and also obscure in one- and two-dimensional spin systems. In fact, the ground-state properties of a spin- $S$  Ising model with the rhombic crystal-field potential  $E$  have been only recently examined by Oitmaa and von Brasch within an effective mapping to the transverse Ising model [6]. On the basis of this effective mapping, the zero-temperature quantum critical point can be exactly located in the one-dimensional model, while for the two-dimensional models, they can be estimated with a high numerical accuracy using the linked-cluster expansion method [6,7]. Nevertheless, the magnetic behaviour of these models has not been investigated at non-zero temperatures beyond the standard mean-field and effective-field theories [8], random phase approximation [9], or above mentioned linked cluster expansion [10]. It should be stressed that the biaxial anisotropy essentially influences the magnetic properties of a large number of polymeric molecular-based magnetic materials, too. From the most obvious examples one could mention:  $\text{NiF}_2$  [11],  $\text{NiNO}_3 \cdot 6\text{H}_2\text{O}$  [12],  $\text{Ni}(\text{CH}_3\text{COO})_2 \cdot 4\text{H}_2\text{O}$  [13],  $\text{Mn}(\text{CH}_3\text{COO})_2 \cdot 3\text{H}_2\text{O}$  [14],  $\text{CoF}_2$  [15],  $\text{CoCl}_2 \cdot 6\text{H}_2\text{O}$  [16] and a series of compounds  $\text{Fe}(\text{dc})_2\text{X}$  [17], where  $\text{X}$  stands for halides and  $\text{dc}$  for the dithiocarbamate or diselenocarbamate groups, respectively.

In this article, we will focus on the effect of uniaxial and biaxial crystal-field potentials affecting the magnetic behaviour of the mixed spin-1/2 and spin-3/2 honeycomb lattice. When assuming an Ising-type exchange interaction between nearest-neighbours, the model becomes exactly solvable within an extended star-triangle mapping transformation. Thus, the considered model provides a noble example of statistical system, which enables to study an interplay between the quantum effects and temperature in a spontaneously ordered magnetic system. Moreover, the magnetic structure of a mixed-spin honey-

comb lattice occurs rather frequently also in the molecular magnetism, what clearly demonstrates a large family of polymeric two-dimensional compounds of following chemical formula:  $A^I M^{II} M^{III} (C_2O_4)_3$  [18], where  $A^I$  stands for a non-magnetic univalent cation  $N(C_n H_{2n+1})_4$  or  $P(C_n H_{2n+1})_4$  ( $n = 3 - 5$ ),  $M^{II}$  and  $M^{III}$  denote two- and three-valent metal atoms  $Cu^{II}(S = 1/2)$ ,  $Ni^{II}(S = 1)$ ,  $Co^{II}(S = 3/2)$ ,  $Fe^{II}(S = 2)$  or  $Mn^{II}(S = 5/2)$  and respectively,  $Cr^{III}(S = 3/2)$  or  $Fe^{III}(S = 5/2)$ . Actually, it turns out that the crystal structure of these polymeric molecular-based magnetic materials consists of the well-separated two-dimensional layers, in which regularly alternating  $M^{II}$  and  $M^{III}$  magnetic metal atoms constitute more or less regular honeycomb lattice (Fig. 1). In consequence of a large magnetocrystalline anisotropy of these materials, one should also expect a relatively strong uniaxial (Ising-like) anisotropy, as it has already been suggested in the theoretical studies based on the effective-field theory and Monte-Carlo simulations [19]. Hence, the magnetic compounds from the family of oxalates  $A^I M^{II} M^{III} (C_2O_4)_3$  represent the good candidates to be described by the proposed model.

The outline of this paper is as follows. In the next section the detailed description of the model system is presented and then, some basic aspects of the transformation method will be shown. Section 3 deals with the physical interpretation of the most interesting results and finally, some concluding remarks are drawn in Section 4.

## 2 Model and method

Let us consider the magnetic structure of a mixed-spin honeycomb lattice, as it is schematically depicted in Fig. 1. To ensure exact tractability of the model system, we will further suppose that the sites of sublattice  $A$  are occupied by the spin-1/2 atoms (depicted as full circles), in contrast to the sites of sublattice  $B$  that are occupied by the spin-3/2 atoms (open circles). Assuming the Ising-type exchange interaction  $J$  between the nearest-neighbouring spin pairs only, the total Hamiltonian of the system reads:

$$\hat{\mathcal{H}} = J \sum_{\langle k,j \rangle} \hat{S}_k^z \hat{\mu}_j^z + D \sum_{k \in B} (\hat{S}_k^z)^2 + E \sum_{k \in B} [(\hat{S}_k^x)^2 - (\hat{S}_k^y)^2], \quad (1)$$

where  $N$  is the total number of sites at each sublattice,  $\hat{\mu}_j^z$  and  $\hat{S}_k^\alpha$  ( $\alpha = x, y, z$ ) denote the standard spatial components of the spin-1/2 and spin-3/2 operators, respectively. The first summation in Eq. (1) is carried out over the nearest-neighbouring spin pairs, while the other two summations run over the sites of sublattice  $B$ . Apparently, the last two terms  $D$  and  $E$  are the crystal-field potentials that measure a strength of uniaxial and biaxial anisotropies

acting on the spin-3/2 atoms. It is also worthy to note that there is one-to-one correspondence between the Hamiltonian (1) and the effective spin Hamiltonian with three different single-ion anisotropy terms  $D^x$ ,  $D^y$  and  $D^z$ :

$$\hat{\mathcal{H}} = J \sum_{\langle k,j \rangle}^{3N} \hat{S}_k^z \hat{\mu}_j^z + D^z \sum_{k \in B}^N (\hat{S}_k^z)^2 + D^x \sum_{k \in B}^N (\hat{S}_k^x)^2 + D^y \sum_{k \in B}^N (\hat{S}_k^y)^2. \quad (2)$$

As a matter of fact, one can easily prove the equivalence between (1) and (2) by the use of the following mapping relations between the relevant interaction parameters:

$$D = D^z - \frac{1}{2}(D^x + D^y), \quad \text{and} \quad E = \frac{1}{2}(D^x - D^y). \quad (3)$$

It should be also mentioned here that by neglecting the biaxial anisotropy, i.e. setting  $E = 0$  in Eq. (1) or equivalently  $D^x = D^y$  in Eq. (2), our model reduces to the exactly soluble model settled by Gonçalves [20]. Accordingly, the main attention will be focused here on the effect of biaxial anisotropy, which influences the thermodynamical and dynamical properties in a crucial manner. Really, the  $E$  term related to the biaxial crystal-field anisotropy should cause non-trivial quantum effects, since it introduces the  $x$  and  $y$  components of spin operators into the Hamiltonian (1). As a result, it is responsible for the onset of local quantum fluctuations that are obviously missing in the Ising model with the uniaxial crystal-field potential  $D$  only.

It is therefore of interest to discuss an origin of the biaxial crystal-field potential  $E$ . The origin of this anisotropy term consists in the low-symmetry crystal field of ligands from the local neighbourhood of the spin-3/2 atoms. It is noticeable that a threefold symmetry axis oriented perpendicular to the honeycomb layer prevents an appearance of biaxial crystal-field potential in a regular honeycomb lattice with a perfect arrangement of the oxalato groups, as well as magnetic metal atoms. However, a small lattice distortion, which occurs rather frequently in the low-dimensional polymeric compounds due to the Jahn-Teller effect, can potentially lower the local symmetry. In consequence of that, the distortion of lattice parameters can be regarded as a possible source of the biaxial crystal-field anisotropy. The most obvious example, where the lattice distortion removes the threefold symmetry axis represents the single-molecule magnet  $\text{Fe}_4$ , in which three outer Fe atoms occupy two non-equivalent positions around one central Fe atom [2].

Let us turn our attention to the main points of the transformation method, which enables an exact treatment of the model system. Firstly, it is very con-

venient to write the total Hamiltonian (1) as a sum of the site Hamiltonians:

$$\hat{\mathcal{H}} = \sum_{k \in B}^N \hat{\mathcal{H}}^{(k)}, \quad (4)$$

where the each site Hamiltonian  $\hat{\mathcal{H}}^{(k)}$  involves all interaction terms associated with one spin-3/2 atom residing on the  $k$ th site of sublattice  $B$ :

$$\hat{\mathcal{H}}^{(k)} = \hat{S}_k^z E_k + (\hat{S}_k^z)^2 D + [(\hat{S}_k^x)^2 - (\hat{S}_k^y)^2] E, \quad (5)$$

with  $E_k = J(\hat{\mu}_{k1}^z + \hat{\mu}_{k2}^z + \hat{\mu}_{k3}^z)$ . While the Hamiltonians (5) at different sites commute with respect to each other ( $[\hat{\mathcal{H}}^{(i)}, \hat{\mathcal{H}}^{(j)}] = 0$ , for each  $i \neq j$ ), the partition function of the system can be partially factorized and consequently, rewritten in the form:

$$\mathcal{Z} = \text{Tr}_{\{\mu\}} \prod_{k=1}^N \text{Tr}_{S_k} \exp[-\beta \hat{\mathcal{H}}^{(k)}]. \quad (6)$$

In above,  $\beta = 1/(k_B T)$ ,  $k_B$  is Boltzmann's constant,  $T$  the absolute temperature,  $\text{Tr}_{\{\mu\}}$  means a trace over spin degrees of freedom of sublattice  $A$  and  $\text{Tr}_{S_k}$  stands for a trace over spin states of the  $k$ th spin from sublattice  $B$ . The crucial step in our procedure represents the calculation of the expression  $\text{Tr}_{S_k} \exp[-\beta \hat{\mathcal{H}}^{(k)}]$ . With regard to this, let us write the site Hamiltonian (5) in an usual matrix representation:

$$\hat{\mathcal{H}}^{(k)} = \begin{pmatrix} \frac{9D}{4} + \frac{3E_k}{2} & 0 & \sqrt{3}E & 0 \\ 0 & \frac{D}{4} + \frac{E_k}{2} & 0 & \sqrt{3}E \\ \sqrt{3}E & 0 & \frac{D}{4} - \frac{E_k}{2} & 0 \\ 0 & \sqrt{3}E & 0 & \frac{9D}{4} - \frac{3E_k}{2} \end{pmatrix}, \quad (7)$$

in a standard basis of functions  $|\pm 3/2\rangle, |\pm 1/2\rangle$  corresponding, respectively, to the four possible spin states  $S_k^z = \pm 3/2, \pm 1/2$  of the  $k$ th atom from sublattice  $B$ . Although it is easy to find eigenvalues of the site Hamiltonian (7), with respect to further calculation it is more favorable to obtain directly the matrix elements of the expression  $\exp[-\beta \hat{\mathcal{H}}^{(k)}]$ . When adopting the Cauchy integral formula, one readily attains the matrix elements for an arbitrary exponential function of the site Hamiltonian (7):

$$A_{ij} = \left( \exp[\alpha \hat{\mathcal{H}}^{(k)}] \right)_{ij},$$

$$\begin{aligned}
A_{11} &= \exp\left[\alpha\left(\frac{5}{4}D + \frac{1}{2}E_k\right)\right]\left\{\cosh(a\xi_k^+) + \frac{D + E_k}{\xi_k^+} \sinh(a\xi_k^+)\right\}, \\
A_{22} &= \exp\left[\alpha\left(\frac{5}{4}D - \frac{1}{2}E_k\right)\right]\left\{\cosh(a\xi_k^-) - \frac{D - E_k}{\xi_k^-} \sinh(a\xi_k^-)\right\}, \\
A_{33} &= \exp\left[\alpha\left(\frac{5}{4}D + \frac{1}{2}E_k\right)\right]\left\{\cosh(a\xi_k^+) - \frac{D + E_k}{\xi_k^+} \sinh(a\xi_k^+)\right\}, \\
A_{44} &= \exp\left[\alpha\left(\frac{5}{4}D - \frac{1}{2}E_k\right)\right]\left\{\cosh(a\xi_k^-) + \frac{D - E_k}{\xi_k^-} \sinh(a\xi_k^-)\right\}, \\
A_{13} &= A_{31} = \exp\left[\alpha\left(\frac{5}{4}D + \frac{1}{2}E_k\right)\right]\frac{\sqrt{3}E}{\xi_k^+} \sinh(a\xi_k^+), \\
A_{24} &= A_{42} = \exp\left[\alpha\left(\frac{5}{4}D - \frac{1}{2}E_k\right)\right]\frac{\sqrt{3}E}{\xi_k^-} \sinh(a\xi_k^-),
\end{aligned} \tag{8}$$

where  $\xi_k^\pm = \sqrt{(D \pm E_k)^2 + 3E^2}$  and  $\alpha$  marks an arbitrary function. After substituting  $\alpha = -\beta$  in the set of Eqs. (8), the calculation of the relevant trace  $\text{Tr}_{S_k} \exp[-\beta \hat{\mathcal{H}}^{(k)}]$  can easily be accomplished. Moreover, its explicit form immediately implies a possibility of performing the standard star-triangle mapping transformation:

$$\begin{aligned}
\text{Tr}_{S_k} \exp[-\beta \hat{\mathcal{H}}^{(k)}] &= 2 \exp[-5\beta D/4 - \beta E_k/2] \cosh\left(\beta \sqrt{(D + E_k)^2 + 3E^2}\right) \\
&\quad + 2 \exp[-5\beta D/4 + \beta E_k/2] \cosh\left(\beta \sqrt{(D - E_k)^2 + 3E^2}\right) = \\
&= A \exp\left[\beta R(\mu_{k1}^z \mu_{k2}^z + \mu_{k2}^z \mu_{k3}^z + \mu_{k3}^z \mu_{k1}^z)\right],
\end{aligned} \tag{9}$$

which replaces the partition function of a *star* (i. e. the four-spin cluster consisting of one central spin-3/2 atom and its three nearest-neighbouring spin-1/2 atoms) by the partition function of a *triangle* (i. e. the three-spin cluster comprising of three outer spin-1/2 atoms in the corners of equilateral triangle), as shown in Fig. 1. The physical meaning of the mapping (9) is to remove all interaction parameters associated with the central spin-3/2 atom and to replace them by the effective interaction  $R$  between the outer spin-1/2 atoms. It is noteworthy that both mapping parameters  $A$  and  $R$  are "self-consistently" given by the transformation equation (9), which must be valid for any combination of spin states of three spin-1/2 atoms. In consequence of that, the transformation parameters  $A$  and  $R$  can be expressed:

$$A = (\Phi_1 \Phi_2^3)^{1/4}, \quad \beta R = \ln\left(\frac{\Phi_1}{\Phi_2}\right), \tag{10}$$

where the functions  $\Phi_1$  and  $\Phi_2$  are defined as follows:

$$\Phi_1 = 2 \exp(-5\beta D/4 - 3\beta J/4) \cosh\left(\beta \sqrt{(3J/2 + D)^2 + 3E^2}\right)$$

$$\begin{aligned}
& + 2 \exp(-5\beta D/4 + 3\beta J/4) \cosh\left(\beta\sqrt{(3J/2 - D)^2 + 3E^2}\right), \\
\Phi_2 = & 2 \exp(-5\beta D/4 - \beta J/4) \cosh\left(\beta\sqrt{(J/2 + D)^2 + 3E^2}\right) \\
& + 2 \exp(-5\beta D/4 + \beta J/4) \cosh\left(\beta\sqrt{(J/2 - D)^2 + 3E^2}\right). \tag{11}
\end{aligned}$$

When the mapping (9) is performed at each site of the sublattice  $B$ , the original mixed-spin honeycomb lattice is mapped onto the spin-1/2 Ising triangular lattice with the effective interaction  $R$  given by the "self-consistency" condition (10)-(11). Indeed, the substitution of equation (9) into the partition function (6) establishes the relationship:

$$\mathcal{Z}(\beta, J, D, E) = A^N \mathcal{Z}_t(\beta, R), \tag{12}$$

between the partition function  $\mathcal{Z}$  of the mixed-spin honeycomb lattice and the partition function  $\mathcal{Z}_t$  of the corresponding spin-1/2 triangular lattice. Above equation constitutes the basic result of our calculation, since it enables relatively simple derivation of all required quantities, such as the magnetization, quadrupolar moment, correlation function, internal energy, specific heat, etc. In addition, by combining (12) with (9) one readily proves the validity of following exact spin identities:

$$\langle f_1(\mu_i^z, \mu_j^z, \dots, \mu_k^z) \rangle = \langle f_1(\mu_i^z, \mu_j^z, \dots, \mu_k^z) \rangle_t, \tag{13}$$

$$\begin{aligned}
\langle f_2(S_k^x, S_k^y, S_k^z, \mu_{k1}^z, \mu_{k2}^z, \mu_{k3}^z) \rangle = \\
= \left\langle \frac{\text{Tr}_{S_k} f_2(S_k^x, S_k^y, S_k^z, \mu_{k1}^z, \mu_{k2}^z, \mu_{k3}^z) \exp[-\beta \hat{\mathcal{H}}^{(k)}]}{\text{Tr}_{S_k} \exp[-\beta \hat{\mathcal{H}}^{(k)}]} \right\rangle, \tag{14}
\end{aligned}$$

where  $\langle \dots \rangle$  represents the standard canonical average over the ensemble defined by the Hamiltonian (1) and  $\langle \dots \rangle_t$  the one performed on the spin-1/2 Ising triangular lattice with the effective exchange interaction  $R$ . Here,  $f_1$  is an arbitrary function of the spin variables belonging to the sublattice  $A$ , while  $f_2$  denotes an arbitrary function depending on the  $k$ th spin of sublattice  $B$  and its three nearest-neighbours from the sublattice  $A$ . Applying the spin identity (13), one straightforwardly attains the following results:

$$m_A \equiv \langle \hat{\mu}_{k1}^z \rangle = \langle \hat{\mu}_{k1}^z \rangle_t \equiv m_t, \tag{15}$$

$$c_A \equiv \langle \hat{\mu}_{k1}^z \hat{\mu}_{k2}^z \rangle = \langle \hat{\mu}_{k1}^z \hat{\mu}_{k2}^z \rangle_t \equiv c_t, \tag{16}$$

$$t_A \equiv \langle \hat{\mu}_{k1}^z \hat{\mu}_{k2}^z \hat{\mu}_{k3}^z \rangle = \langle \hat{\mu}_{k1}^z \hat{\mu}_{k2}^z \hat{\mu}_{k3}^z \rangle_t \equiv t_t, \tag{17}$$

whereas the second spin identity (14) enables after some algebra derivation of quantities depending on the spin variable from the sublattice  $B$ :

$$m_B \equiv \langle \hat{S}_k^z \rangle = -3m_A(K_1 + K_2)/2 - 2t_A(K_1 - 3K_2), \quad (18)$$

$$\eta \equiv \langle (\hat{S}_k^z)^2 \rangle = (K_3 + 3K_4)/4 + 3c_A(K_3 - K_4). \quad (19)$$

In above,  $m_A$  ( $m_B$ ) labels the single-site magnetization of the sublattice  $A$  ( $B$ ),  $\eta$  denotes the quadrupolar moment and finally,  $c_A$  and  $t_A$  stand, respectively, for the static pair and triplet correlation functions between the relevant spins of sublattice  $A$ . Obviously, the exact solution of both the sublattice magnetization and quadrupolar moment require only the knowledge of the single-site magnetization  $m_t$ , nearest-neighbour pair correlation function  $c_t$  and triplet correlation function  $t_t$  on the corresponding spin-1/2 Ising triangular lattice unambiguously given by  $R$  (10)-(11). Fortunately, the appropriate exact solution of these quantities is well known, hence, one can directly utilize the final results derived in Refs. [21]. Finally, the coefficients emerging in the previous set of Eqs. (17)-(20) are listed below:

$$\begin{aligned} K_1 &= F_1(3J/2 + D, 3J/2 - D, 3J/2), \quad K_2 = F_1(J/2 + D, J/2 - D, J/2), \\ K_3 &= F_2(3J/2 + D, 3J/2 - D, 3J/2), \quad K_4 = F_2(J/2 + D, J/2 - D, J/2), \end{aligned} \quad (20)$$

where the functions  $F_1(x, y, z)$  and  $F_2(x, y, z)$  are defined as follows:

$$\begin{aligned} F_1(x, y, z) &= \frac{x}{\sqrt{x^2 + 3E^2}} \frac{\sinh(\beta\sqrt{x^2 + 3E^2})}{\cosh(\beta\sqrt{x^2 + 3E^2}) + \exp(\beta z) \cosh(\beta\sqrt{y^2 + 3E^2})} \\ &+ \frac{y}{\sqrt{y^2 + 3E^2}} \frac{\sinh(\beta\sqrt{y^2 + 3E^2})}{\exp(-\beta z) \cosh(\beta\sqrt{x^2 + 3E^2}) + \cosh(\beta\sqrt{y^2 + 3E^2})} \\ &- \frac{1}{2} \frac{\cosh(\beta\sqrt{x^2 + 3E^2}) - \exp(\beta z) \cosh(\beta\sqrt{y^2 + 3E^2})}{\cosh(\beta\sqrt{x^2 + 3E^2}) + \exp(\beta z) \cosh(\beta\sqrt{y^2 + 3E^2})}, \\ F_2(x, y, z) &= \frac{y}{\sqrt{y^2 + 3E^2}} \frac{\sinh(\beta\sqrt{y^2 + 3E^2})}{\exp(-\beta z) \cosh(\beta\sqrt{x^2 + 3E^2}) + \cosh(\beta\sqrt{y^2 + 3E^2})} \\ &+ \frac{5}{4} - \frac{x}{\sqrt{x^2 + 3E^2}} \frac{\sinh(\beta\sqrt{x^2 + 3E^2})}{\cosh(\beta\sqrt{x^2 + 3E^2}) + \exp(\beta z) \cosh(\beta\sqrt{y^2 + 3E^2})}. \end{aligned} \quad (21)$$

Now, we will derive exact result for one dynamical quantity, namely, the time-dependent autocorrelation function. It should be noted here that the exactly tractable models offer only seldom the possibility to investigate their spin dynamics. On the other hand, the dynamical quantities such as autocorrelation and correlation functions are important also from the experimental point of view, because their magnitude directly determines the scattering cross section measured in an inelastic neutron scattering experiments [22], or the spin-lattice relaxation rate provided by the nuclear magnetic resonance technique [23].



As a starting point for the calculation of the time-dependent autocorrelation function  $C_{auto}^{zz}$  can, for convenience, serve the exact spin identity (14):

$$\begin{aligned} C_{auto}^{zz}(t) &\equiv \frac{1}{2} \langle \hat{S}_k^z(0) \hat{S}_k^z(t) + \hat{S}_k^z(t) \hat{S}_k^z(0) \rangle = \\ &= \frac{1}{2} \left\langle \frac{\text{Tr}_{S_k} \{ [\hat{S}_k^z(0) \hat{S}_k^z(t) + \hat{S}_k^z(t) \hat{S}_k^z(0)] \exp[-\beta \hat{\mathcal{H}}^{(k)}] \}}{\text{Tr}_{S_k} \exp[-\beta \hat{\mathcal{H}}^{(k)}]} \right\rangle, \end{aligned} \quad (22)$$

where the symmetrized form in the definition of  $C_{auto}^{zz}$  is used to construct a Hermitian operator,  $\hat{S}_k^z(t) = \exp(\frac{it\hat{\mathcal{H}}_k}{\hbar}) \hat{S}_k^z \exp(-\frac{it\hat{\mathcal{H}}_k}{\hbar})$  represents the Heisenberg picture for the time-dependent operator  $\hat{S}_k^z(t)$ ,  $\hbar$  stands for the reduced Planck's constant and  $i = \sqrt{-1}$ . Next, the matrix elements of the expressions  $\exp(\pm \frac{it\hat{\mathcal{H}}_k}{\hbar})$  can be in turn evaluated by putting  $\alpha = \pm \frac{it}{\hbar}$  into the set of Eqs. (8). Then, after a straightforward but a little bit tedious calculation, one arrives to the final result for the dynamical autocorrelation function:

$$\begin{aligned} C_{auto}^{zz} &= \frac{1}{4} [K_5(D + 3J/2, D - 3J/2, 3J/2) + 3K_6(D + J/2, D - J/2, J/2)] \\ &+ 3c_t [K_5(D + 3J/2, D - 3J/2, 3J/2) - K_6(D + J/2, D - J/2, J/2)], \end{aligned} \quad (23)$$

where the coefficients  $K_5$  and  $K_6$  are explicitly given in the Appendix.

### 3 Results and discussion

Before proceeding to the discussion of the most interesting results, it is noticeable that the results derived in the previous section are rather general, since they are valid for the ferromagnetic ( $J < 0$ ), as well as ferrimagnetic ( $J > 0$ ) version of the model under investigation. In what follows, we will restrict ourselves to the analysis of the ferrimagnetic model only, since the polymeric compounds from the family of oxalates [18] fall mostly into the class of ferrimagnets. Nevertheless, it appears worthwhile to remark that the magnetic behaviour of the ferrimagnetic system completely resembles that one of the ferromagnetic system. Finally, one should also emphasize that the mapping (9) remains invariant under the transformation  $E \leftrightarrow -E$ . For this reason, one may consider without loss of generality the parameter  $E \geq 0$  and consequently,  $x$ -,  $y$ - and  $z$ -axis then represent the hard-, medium- and easy-axis for a given system.

### 3.1 Ground-state properties

At first, we will take a closer look at the ground-state behaviour. Taking into account the zero-temperature limit ( $T \rightarrow 0^+$ ), one finds the following condition for a first-order phase transition line separating two different magnetically ordered phases denoted as OP<sub>1</sub> and OP<sub>2</sub>:

$$\frac{D}{J} = \sqrt{\left(\frac{3}{4}\right)^2 + \left(\frac{E}{J}\right)^2}. \quad (24)$$

Moreover, one easily attains from Eqs. (15)-(21) analytical results for the single-site sublattice magnetization ( $m_A, m_B$ ), the total magnetization normalized per one magnetic atom  $m = (m_A + m_B)/2$  and the quadrupolar moment  $\eta$ , as well:

$$\text{OP}_1: \quad m_A = -\frac{1}{2}, \quad m_B = \frac{1}{2} + \frac{\frac{3}{2} - \frac{D}{J}}{\sqrt{\left(\frac{3}{2} - \frac{D}{J}\right)^2 + 3\left(\frac{E}{J}\right)^2}}, \quad (25)$$

$$m = \frac{1}{2} \frac{\frac{3}{2} - \frac{D}{J}}{\sqrt{\left(\frac{3}{2} - \frac{D}{J}\right)^2 + 3\left(\frac{E}{J}\right)^2}}, \quad \eta = \frac{5}{4} + \frac{\frac{3}{2} - \frac{D}{J}}{\sqrt{\left(\frac{3}{2} - \frac{D}{J}\right)^2 + 3\left(\frac{E}{J}\right)^2}};$$

$$\text{OP}_2: \quad m_A = -\frac{1}{2}, \quad m_B = -\frac{1}{2} + \frac{\frac{3}{2} + \frac{D}{J}}{\sqrt{\left(\frac{3}{2} + \frac{D}{J}\right)^2 + 3\left(\frac{E}{J}\right)^2}}, \quad (26)$$

$$m = -\frac{1}{2} - \frac{1}{2} \frac{\frac{3}{2} - \frac{D}{J}}{\sqrt{\left(\frac{3}{2} - \frac{D}{J}\right)^2 + 3\left(\frac{E}{J}\right)^2}}, \quad \eta = \frac{5}{4} - \frac{\frac{3}{2} + \frac{D}{J}}{\sqrt{\left(\frac{3}{2} + \frac{D}{J}\right)^2 + 3\left(\frac{E}{J}\right)^2}}.$$

For better illustration, Fig. 2 depicts the ground-state phase diagram in the  $E$ - $D$  plane (Fig. 2a) and the zero-temperature variations of the magnetization and quadrupolar moment with the biaxial anisotropy when  $D/J = 1.0$  (Fig. 2b). It should be also mentioned that by neglecting the biaxial anisotropy, i.e. by putting  $E/J = 0.0$  into the phase boundary condition (24), one recovers the boundary uniaxial anisotropy  $D/J = 0.75$  in accordance with the results reported by Gonçalves several years ago [20]. Moreover, the OP<sub>1</sub> (OP<sub>2</sub>) phase corresponds in this limit to the simple ferrimagnetic (antiferromagnetic) phase with both the sublattice magnetization oriented antiparallel with respect to each other:  $m_A = -0.5$ ,  $m_B = 1.5$  in the OP<sub>1</sub> and respectively,  $m_A = -0.5$ ,  $m_B = 0.5$  in the OP<sub>2</sub>. Apparently, the spin-3/2 atoms occupy exclusively the  $|+3/2\rangle$  ( $|+1/2\rangle$ ) in the OP<sub>1</sub> (OP<sub>2</sub>) phase, when  $E = 0$  is satisfied.

The situation becomes much more complex by turning on the biaxial anisotropy. Even though the sublattice magnetization  $m_A$  remains in the ground-state at its saturation value in both the  $OP_1$  and  $OP_2$  phases, the sublattice magnetization  $m_B$  is gradually suppressed by the effect of biaxial anisotropy (see Fig. 2b). It is quite obvious from this figure that the biaxial anisotropy gradually destroys the perfect ferrimagnetic (antiferromagnetic) spin arrangement, which occurs in the  $OP_1$  ( $OP_2$ ) phase in the limit of vanishing  $E$ . Let us find a primary occasion for this unexpected behaviour accompanied by a spin reduction at sublattice  $B$ . According to Eq. (26), one finds  $\eta - m_B = 3/4$  to be valid in the whole parameter space corresponding to the  $OP_1$ . From an elementary consideration it can be easily understood that the spin-3/2 atoms occupy in the  $OP_1$  phase either the  $|+3/2\rangle$  or  $|-1/2\rangle$  state, in order to satisfy simultaneously both the ground-state values for  $m_B$  and  $\eta$ . Aforementioned argument is also supported by the fact, that the  $E$  term does not couple in the Hamiltonian (7) the  $|+3/2\rangle$  and  $|-1/2\rangle$  states with the  $|+1/2\rangle$  and  $|-3/2\rangle$  ones. Hence, the  $|+3/2\rangle$  and  $|-1/2\rangle$  states are in the  $OP_1$  phase the only *allowable* states, while the  $|+1/2\rangle$  and  $|-3/2\rangle$  states are, on the contrary, the *forbidden* ones. The observed spin reduction at sublattice  $B$  can be thus attributed to the local quantum fluctuations induced by the biaxial anisotropy, which in turn lead to a spin tunneling between the  $|+3/2\rangle$  and  $|-1/2\rangle$  states in the  $OP_1$ . Although the occupation of the minority  $|-1/2\rangle$  state rises steadily with increasing the biaxial anisotropy strength, it is noticeable that the  $|+3/2\rangle$  state still remains the state with the most probable occupation. For completeness, it should be pointed out that in accord with our expectation the negative uniaxial anisotropy ( $D < 0$ ) reduces the occupation of the minority  $|-1/2\rangle$  state, while the positive one ( $D > 0$ ) prefers it.

Quite similar situation emerges also in the  $OP_2$  phase. However, it is worth while to remark that the  $OP_2$  phase appears in a region of the uniaxial anisotropies  $D/J > 0.75$  only. Due to strong positive uniaxial anisotropy, the spin-3/2 atoms undergo a well-known spin transition from the  $|+3/2\rangle$  to  $|+1/2\rangle$  state, which macroscopically manifests itself in the phase transition from the  $OP_1$  to  $OP_2$  phase. Nevertheless, as stated before, the biaxial anisotropy couples together the  $|+1/2\rangle$  state with the  $|-3/2\rangle$  one, hence, the tunneling between these spin states should be expected to occur in the  $OP_2$ . The analytical solution for  $m_B$  and  $\eta$  (27), as well as a validity of the relation  $\eta + m_B = 3/4$  in the whole parameter space corresponding to the  $OP_2$  phase, indeed confirm this suggestion. However, the negative (positive) uniaxial anisotropy prefers (reduces) in the  $OP_2$  phase the occupation of the minority  $|-3/2\rangle$  state contrary to the situation observed in the  $OP_1$  phase.

Now, let us step forward to the discussion of the time dependent autocorrelation function (23). This quantity can, among other matters, serve in evidence whether the spin-3/2 atoms fluctuate in the  $OP_1$  ( $OP_2$ ) phase between their *allowable*  $|+3/2\rangle$  and  $|-1/2\rangle$  ( $|+1/2\rangle$  and  $|-3/2\rangle$ ) spin states. Unfortunately,

it is quite tedious to derive from Eq. (23) a simple analytical expression for  $C_{auto}^{zz}$  in the zero-temperature limit, hence, we report for  $C_{auto}^{zz}$  numerical results obtained at very low temperature ( $k_B T/J = 0.001$ ) close to the ground state. Fig. 3 displays the time variation of  $C_{auto}^{zz}$  for several values of uniaxial and biaxial crystal-field potentials. Since  $C_{auto}^{zz}$  evidently varies in time, it clearly demonstrates the zero-temperature spin dynamics between the *allowable* states. Moreover, the detailed analysis reveals that  $C_{auto}^{zz}$  is in the zero-temperature limit a harmonic function of time and whence, the time dependence can be characterized by an angular frequency  $\omega_{\pm} = \frac{2J}{\hbar} \sqrt{(\frac{D}{J} \pm 1) + 3(\frac{E}{J})^2}$  depending on whether the system resides the OP<sub>1</sub>, or OP<sub>2</sub> phase. This result is taken to mean that the spin system necessarily recovers after some characteristic recurrence time ( $\tau_{\pm} = 2\pi/\omega_{\pm}$ ) its initial state. More specifically, Fig. 3a illustrates the time variation of  $C_{auto}^{zz}$  in the OP<sub>1</sub> phase, because with respect to Eq. (24) one never approaches the OP<sub>2</sub> phase for  $D/J = 0.0$ . Fig. 3a clearly clarifies the role of biaxial anisotropy: the stronger the biaxial anisotropy  $E/J$ , the greater the angular frequency of spin tunneling and in the consequence of that, the shorter the appropriate recurrence time. Furthermore, the increasing strength of the biaxial anisotropy enhances also the amplitude of oscillation in the time-dependence of  $C_{auto}^{zz}$ . This observation would suggest that the increase of biaxial anisotropy enhances the number of the spin-3/2 atoms tunneling during the recurrence time between the  $|+3/2\rangle$  and  $|-1/2\rangle$  states in the OP<sub>1</sub> phase. However, since the equilibrium magnetization does not change in time, the number of atoms that tunnel from  $|+3/2\rangle$  to  $|-1/2\rangle$  state must definitely be the same as the number of atoms that tunnel from the  $|-1/2\rangle$  to  $|+3/2\rangle$  state.

To illustrate the effect of uniaxial anisotropy, the time variation of  $C_{auto}^{zz}$  is shown in Fig. 3b for  $E/J = 0.5$  and several values of  $D/J$ . Apparently, the  $C_{auto}^{zz}$  oscillates for strong negative (positive) uniaxial constants  $D/J$  in the vicinity of the boundary values  $C_{auto}^{zz} = 2.25(0.25)$ . These values clearly demonstrate that the prevailing number of spin-3/2 atoms occupy in the OP<sub>1</sub> (OP<sub>2</sub>) phase the  $|+3/2\rangle$  ( $|+1/2\rangle$ ) state, since  $C_{auto}^{zz} = \eta$  when  $t = 0$ . Moreover, the stronger the uniaxial anisotropy (independently of its sign), the smaller the relevant amplitudes of oscillation, i. e. the smaller the number of tunneling atoms during the recurrence time. On the other hand, the increasing strength of uniaxial anisotropy enhances the angular frequency of the oscillation, what means, that the tunneling atoms return from the minority  $|-1/2\rangle$  ( $|-3/2\rangle$ ) state to the most probable occupied  $|+3/2\rangle$  ( $|+1/2\rangle$ ) state of the OP<sub>1</sub> (OP<sub>2</sub>) phase after a shorter recurrence time.

### 3.2 Finite-temperature behaviour

In this part, we would like to comment on the finite-temperature behaviour of the system under investigation. Let us begin by considering the effect of uniaxial and biaxial single-ion anisotropies on the critical behaviour. For this purpose, two typical finite-temperature phase diagrams are illustrated in Fig. 4a and 4b. In both figures, the  $OP_1$  ( $OP_2$ ) phase can be located below the phase boundaries depicted as solid (dashed) lines, while above these boundary lines the usual paramagnetic phase becomes stable. Further, open circles represent special critical points at which both the  $OP_1$  and  $OP_2$  phases coexist. Actually, we have not found any phase transition between the  $OP_1$  and  $OP_2$  phases at non-zero temperatures, what indicates that the  $OP_1$  phase coexists with the  $OP_2$  one at non-zero temperatures merely for the same  $D/J - E/J$  values, as in the ground state (24). Finally, a closer mathematical analysis reveals that both the temperature-driven phase transitions that are related to the  $OP_1$  and  $OP_2$  phase, respectively, are of the second-order and belong to the standard Ising universality class.

Fig. 4a shows the critical temperature ( $T_c$ ) as a function of the uniaxial anisotropy for several values of the biaxial anisotropy. The dependence critical temperature versus uniaxial anisotropy is quite obvious for  $E/J = 0.0$ , when increasing  $D/J$ ,  $T_c$  monotonically decreases. Hence, the critical temperature approaches in the limit  $D/J \rightarrow -\infty(+\infty)$  its minimum (maximum) value  $k_B T_c/J = 0.3796\dots (1.1389\dots)$  in agreement with the exact  $T_c$  (triple  $T_c$ ) of the spin-1/2 Ising honeycomb lattice. The gradual decline of the transition temperature can obviously be explained as a consequence of the fact, that the positive uniaxial anisotropy energetically favors the low-spin  $|\pm 1/2\rangle$  states before the high-spin  $|\pm 3/2\rangle$  ones. The most interesting finding to emerge here is that the biaxial anisotropy may significantly modify the critical behaviour of the studied system. As a matter of fact,  $T_c$  firstly reaches its local minimum at certain positive  $D/J$  and then rises steadily to its limiting value  $k_B T_c/J = 0.3796\dots$ . The extraordinary increase of  $T_c$  in the region  $D/J > 1.0$  can be explained through the suppression of the occupation of minority  $|-3/2\rangle$  state, which appears in the  $OP_2$  phase due to the uniaxial anisotropy effect. In accordance with previous assumption, the greater the biaxial anisotropy (i.e. the greater the number of atoms that occupy the minority  $|-3/2\rangle$  state), the more impressive increase of  $T_c$  can be observed. In addition, it is easy to understand from here that the biaxial anisotropy substantially lowers the critical temperature of the  $OP_1$  phase in the  $D/J \leq 0.0$  region, in that it is responsible for the quantum spin tunneling between the  $|+3/2\rangle$  and  $|-1/2\rangle$  spin states.

To illustrate the influence of the biaxial anisotropy on the critical behaviour, the dependence of transition temperature on the biaxial anisotropy is shown

in Fig. 4b for several values of the uniaxial anisotropy  $D/J$ . As one would expect,  $T_c$  gradually decreases with increasing the biaxial anisotropy for any  $D/J < 0.75$ . It is quite obvious that the appropriate suppression of  $T_c$  can be attributed to the quantum fluctuations, which become the stronger, the greater the ratio  $E/J$ . Apart from this rather trivial finding, one also observes here the peculiar dependences with the non-monotonic behaviour of  $T_c$ . The critical temperature may exhibit only a slight variation with increasing  $E/J$  (as it is in the case of  $D/J = 1.0$ ), or it may show unexpected local minima, as it is in the case of  $D/J = 2.0$  and  $3.0$ . Since the local minima can be located very near to the coexistence point of the  $OP_1$  and  $OP_2$  phases (depicted as open circles), the relevant increase of  $T_c$  can be related to the  $OP_2 \rightarrow OP_1$  phase transition. Namely, the most populated  $|+1/2\rangle$  spin state in the  $OP_2$  is replaced after this phase transition by the  $|+3/2\rangle$  state, which is the most occupied spin state in the  $OP_1$ . The spin crossover from the low-spin  $|+1/2\rangle$  to the high-spin  $|+3/2\rangle$  state must lead, of course, to a slight increase of  $T_c$ .

At this stage, let us provide an independent check of the critical behaviour by studying the thermal dependences of magnetization. The single-site magnetization against the temperature are plotted in Fig. 5 for the biaxial anisotropy  $E/J = 0.5$  and several values of the uniaxial anisotropy  $D/J$ . Fig. 5a shows a typical situation observed in the  $OP_1$  phase: the more positive the uniaxial crystal-field potential  $D/J$ , the stronger the spin reduction (the lower the magnetization  $m_B$ ) due to the  $|+3/2\rangle \leftrightarrow |-1/2\rangle$  spin tunneling. In consequence of that, the total magnetization alters from the standard Q-type dependence observed for  $D \leq 0$  (see for instance the curves for  $D/J = -2.0$  and  $0.0$ ) to the more interesting R-type dependence, which occurs for positive uniaxial anisotropies ( $D/J = 0.5$  and  $0.75$ ). Unusual slope in the thermal dependence of total magnetization can be related to the more rapid thermal variation of  $m_B$ . In fact, on account of the quantum fluctuations  $m_B$  is thermally easier disturbed than  $m_A$  that, on the contrary, always exhibits the standard Q-type behaviour (spin-1/2 atoms are not directly affected by the biaxial crystal-field potential  $E$ ). Furthermore, Fig. 5b shows how the situation changes by considering the transition toward the  $OP_2$  phase. Actually, both magnetically ordered phases  $OP_1$  and  $OP_2$  have the same internal energy (coexist together) at  $D/J = \sqrt{13}/4$  when  $E/J = 0.5$ , while the  $OP_2$  phase becomes more stable whenever  $D/J > \sqrt{13}/4$ . Accordingly, Fig. 4b displays the thermal variation of sublattice magnetization exactly at the  $OP_1$ - $OP_2$  phase boundary and in the  $OP_2$  phase ( $D/J = 1.0$  and  $1.5$ ). The corresponding thermal dependences of the total magnetization are plotted in the insert of Fig. 5b. As it is apparent from these figures, the initial value of  $m_B$  is suppressed from its saturation value ( $m_B = 0.5$ ) owing to the presence of the minority  $|-3/2\rangle$  state. Nevertheless, a large number of spins can be thermally excited into the  $|+3/2\rangle$  state for the uniaxial anisotropy  $D/J$  from the vicinity of  $OP_1$ - $OP_2$  phase boundary and hence,  $m_B$  rapidly increases upon heating (see the curve for  $D/J = 1.0$ ). As a result of this thermal excitation, the total magnetization

exhibits N-type dependence with one compensation point in which  $m_A$  and  $m_B$  completely cancel out (see the insert in Fig. 5b). Finally, even for stronger uniaxial anisotropies (e.g.  $D/J = 1.5$ ) the total magnetization recovers the Q-shape, since the thermal fluctuations prefer excitations to the  $|-1/2\rangle$  state rather than to the  $|+3/2\rangle$  one. Such a thermal excitation must, naturally, lower the sublattice magnetization  $m_B$ .

To conclude our discussion devoted to the finite-temperature properties, let us proceed to the time variation of the dynamical autocorrelation function  $C_{auto}^{zz}$  as depicted in Fig. 6 for  $E/J = 0.5$  and three selected values of  $D/J$ . In order to enable a comparison between the displayed data at various  $D/J$ , the relevant temperatures are normalized with respect to their appropriate critical temperatures, i.e. we have defined the dimensionless temperature  $\tau = T/T_c$  that measures the difference from the critical point ( $\tau_c = 1.0$ ). The time variations of the  $C_{auto}^{zz}$  from Fig. 6a and 6b display the relevant changes of the dynamical autocorrelation function in the OP<sub>1</sub> phase, while Fig. 6c shows the corresponding dependences in the OP<sub>2</sub> phase. It can be easily understood that  $C_{auto}^{zz}$  is not in general the time-periodic function at non-zero temperatures no matter whether considering  $C_{auto}^{zz}$  in the OP<sub>1</sub>, or OP<sub>2</sub> phase. In fact,  $C_{auto}^{zz}$  arises according to Eq. (23) as a superposition of two harmonic oscillations with two different angular frequencies  $\omega_{\pm} = \frac{2J}{\hbar} \sqrt{(\frac{D}{J} \pm 1)^2 + 3(\frac{E}{J})^2}$  and also various amplitudes. The interference between these harmonic oscillations gives rise to a rather complex time variation of  $C_{auto}^{zz}$ , which is in general aperiodic, displaying nodes and other typical interference effects. The periodicity of  $C_{auto}^{zz}$  at non-zero temperatures is maintained only for some particular  $E/J - D/J$  values, which retain the ratio  $\omega_+/\omega_-$  to be rational, while in any other case,  $C_{auto}^{zz}$  behaves aperiodically.

The dependences drawn in Fig. 6 nicely illustrate also the temperature effect on the spin dynamics. It follows from these dependences that some amplitudes are suppressed as the temperature increases, while another ones become more robust. Obviously, in the high-temperature regime that amplitudes become dominant, which coincide to the oscillation with lower angular frequency. Contrary to this, the amplitudes arising from higher frequency oscillation dominate in the low-temperature regime. The most miscellaneous time variation of  $C_{auto}^{zz}$  thus emerges in the vicinity of critical temperature ( $\tau \approx 1.0$ ), which represents an intermediate temperature range between the low- and high-temperature regime. However, rather exceptional case is displayed in Fig. 6c, where the most miscellaneous dependence appears surprisingly at substantially lower temperature ( $\tau = 0.25$ ) rather than the critical one ( $\tau_c = 1.0$ ). When looking back to the thermal variation of magnetization depicted in Fig. 5b, one finds a feasible explanation for this striking behaviour. It turns out that the temperature ( $\tau \approx 0.25$ ) of the most miscellaneous time variation of  $C_{auto}^{zz}$  coincides with the temperature  $k_B T/J \approx 0.1$ , at which the most robust spin excitation to the  $|+3/2\rangle$  can be observed. In addition to the *allowable*  $|+1/2\rangle$

and  $|-3/2\rangle$  states, the large number of spin-3/2 atoms is therefore thermally excited also to the  $|+3/2\rangle$  spin state. This observation would suggest that the spin excitations can basically modify the spin dynamics as well.

## 4 Concluding remarks

In this article, the exact solution of the mixed spin-1/2 and spin-3/2 Ising model on honeycomb lattice is presented and discussed in detail. The particular attention has been focused on the effect of uniaxial and biaxial crystal-field anisotropies acting on the spin-3/2 atoms. As it has been shown, the presence of the biaxial anisotropy significantly modifies the magnetic behaviour of the system under investigation. It turns out that already a small amount of the biaxial anisotropy raises a non-trivial spin dynamics and basically influences the thermodynamic properties, as well.

The most striking finding to emerge here constitutes an exact evidence of the spin tunneling between the  $|\pm 3/2\rangle$  and  $|\mp 1/2\rangle$  states in two different magnetically ordered phases  $OP_1$  and  $OP_2$ , respectively. Macroscopically, the tunneling effect decreases the critical temperature of the magnetically ordered phases and appreciably suppresses the magnetization of spin-3/2 sublattice. This quantum reduction appears apparently due to the local quantum fluctuations arising from the biaxial crystal-field potential.

There is an interesting correspondence between the model described by the Hamiltonian (1) and a similar model with a local transverse magnetic field  $H^x$  acting on the spin-3/2 atoms only [24]. However, similarity in their actual properties is not accidental, in fact, when neglecting the uniaxial crystal-field potential  $D$  in Hamiltonian (1), an effective mapping  $E \leftrightarrow H^x$  ensures the equivalence between both the models. Since this mapping is not related to the magnetic structure in any fashion, the appropriate correspondence can be extended to the several lattice models. It is therefore valuable to mention that magnetic properties of the models with a local transverse field become a subject matter of many theoretical works [25]. Apparently, the magnetic behaviour of these systems should completely resemble that one of their counterparts with the biaxial crystal-field potential.

Finally, let us turn back to the origin of biaxial anisotropy. Uprise of this anisotropy term in the mixed-spin honeycomb lattice is, namely, closely associated with at least small lattice distortion. To simplify the situation, the proposed Hamiltonian (1) accounts the biaxial crystal-field anisotropy, while a difference between exchange interactions in the different spatial directions has been for simplicity omitted. Nevertheless, the developed procedure can be generalized also to an anisotropic model accounting the different interactions



along various spatial directions in a rather straightforward way. Moreover, the biaxial anisotropy can be even considered as an arbitrary function (linear, quadratic, exponential, logarithmic, ...) of the ratio between appropriate interaction parameters. Hence, it would be very interesting to find out whether such a system is instable toward the spontaneous lattice distortion caused by the spin-Peierls phenomenon. In this direction continues our next work.

## 5 Appendix

An explicit form of the coefficients  $K_5$  and  $K_6$  is given by:

$$K_5(x, y, z) = G(x, y, z)/\Phi_1, \quad \text{and} \quad K_6(x, y, z) = G(x, y, z)/\Phi_2,$$

where the function  $G(x, y, z)$  is defined as follows:

$$\begin{aligned} G(x, y, z) &= \frac{9}{4}[W_1(x)H_1(x, z) + W_1(y)H_1(y, -z)] + \frac{1}{4}[W_2(x)H_2(x, z) \\ &\quad + W_2(y)H_2(y, -z)] - [W_3(x)H_3(x, z) + W_3(y)H_3(y, -z)], \\ W_1(x) &= \left\{ x^2 + E^2 \left[ 1 + 2 \cos(2t\sqrt{x^2 + 3E^2}/\hbar) \right] \right\} / (x^2 + 3E^2), \\ W_2(x) &= \left\{ x^2 - 3E^2 \left[ 1 - 2 \cos(2t\sqrt{x^2 + 3E^2}/\hbar) \right] \right\} / (x^2 + 3E^2), \\ W_3(x) &= \left\{ \sqrt{3}Ex \left[ 1 - \cos(2t\sqrt{x^2 + 3E^2}/\hbar) \right] \right\} / (x^2 + 3E^2), \\ H_1(x, y) &= \exp(-5\beta D/4 - \beta y/2) \left[ \cosh(\beta\sqrt{x^2 + 3E^2}) \right. \\ &\quad \left. - x \sinh(\beta\sqrt{x^2 + 3E^2})/\sqrt{x^2 + 3E^2} \right], \\ H_2(x, y) &= \exp(-5\beta D/4 - \beta y/2) \left[ \cosh(\beta\sqrt{x^2 + 3E^2}) \right. \\ &\quad \left. + x \sinh(\beta\sqrt{x^2 + 3E^2})/\sqrt{x^2 + 3E^2} \right], \\ H_3(x, y) &= \exp(-5\beta D/4 - \beta y/2) \sqrt{3}E \sinh(\beta\sqrt{x^2 + 3E^2})/\sqrt{x^2 + 3E^2}. \end{aligned}$$

## References

- [1] R. Sessoli and D. Gatteschi, *Angew. Chem.* 42 (2003) 268.
- [2] A. L. Barra, A. Caneschi, A. Cornia, F. Fabrizi de Biani, D. Gatteschi, C. Sangregorio, R. Sessoli and L. Sorace, *J. Am. Chem. Soc.* 121 (1999) 5302;  
G. Amoretti, S. Carretta, R. Caciuffo, H. Casalta, A. Cornia, M. Affronte, D. Gatteschi, *Phys. Rev. B* 64 (2001) 104403.

- [3] K. Wieghardt, K. Pohl, I. Jibril, G. Huttner, *Angew. Chem.* 96 (1984) 63;  
M. Hennion, L. Pardi, I. Mirebeau, E. Suard, R. Sessoli, A. Caneschi,  
*Phys. Rev. B* 56 (1997) 8819;  
R. Sessoli, D. Gatteschi, A. Caneschi, M. A. Novak, *Nature* 365 (1993) 141;  
R. Sessoli, *Mol. Cryst. Liq. Cryst.* 274 (1995) 145.
- [4] J. C. Goodwin, R. Sessoli, D. Gatteschi, W. Wernsdorfer, A. K. Powell and  
S. L. Heath, *J. Chem. Soc. Dalton Trans.* (2000) 1835;  
M. Affronte, J. C. Lasjaunias, W. Wernsdorfer, R. Sessoli, D. Gatteschi,  
S. L. Heath, A. Fort and A. Rettori, *Phys. Rev. B* 66 (2002) 064408.
- [5] W. Wernsdorfer, S. Bhaduri, C. Boskovic, G. Christou and D. N. Hendrickson,  
*Phys. Rev. B* 65 (2002) 180403.
- [6] J. Oitmaa and A. M. A. von Brasch, *Phys. Rev. B* 67 (2003) 172402.
- [7] K. K. Pan and Y.-L. Wang, *Phys. Rev. B* 51 (1995) 3610.
- [8] N. Ch. Eddeqaqi, M. Saber, A. El-Atri and M. Kerouad,  
*Physica A* 272 (1999) 144;  
W. Jiang, G. Z. Wei and A. Du, *J. Magn. Magn. Mater.* 250 (2002) 49;  
W. Jiang, G. Z. Wei, A. Du and L. Q. Guo, *Physica A* 313 (2002) 503;  
W. Jiang, G. Z. Wei and Q. Zhang, *Physica A* 329 (2003) 161.
- [9] G. P. Taggart, R. A. Tahir-Kheli and E. Shiles, *Physica* 75 (1974) 234;  
R. Mienas, *Physica A* 89 (1977) 431.
- [10] K. K. Pan and Y.-L. Wang, *Phys. Lett. A* 178 (1993) 325.
- [11] T. Moriya, *Phys. Rev.* 117 (1960) 635.
- [12] L. Berger and S. A. Friedberg, *Phys. Rev.* 136 (1964) A158.
- [13] L. G. Polgar and S. A. Friedberg, *Phys. Rev. B* 6 (1972) 3497.
- [14] H. Kumagai, K. Ôno, I. Hayashi and K. Kambe, *Phys. Rev.* 2 (1952) 374.
- [15] M. E. Lines, *Phys. Rev.* 137 (1965) A982.
- [16] N. Uryû, J. Skalyo and S. A. Friedberg, *Phys. Rev.* 144 (1966) 684.
- [17] G. C. DeFotis, F. Palacio and R. L. Carlin, *Phys. Rev. B* 20 (1979) 2945;  
G. C. De Fotis, B. K. Failon, F. V. Wells and H. H. Wickman,  
*Phys. Rev. B* 29 (1984) 3795.
- [18] Z. J. Zhong, N. Matsumoto, H. Ôkawa, S. Kida, *Chem. Lett.* (1990) 87;  
H. Tamaki, M. Mitsumi, K. Nakamura, N. Matsumoto, S. Kida, H. Ôkawa and  
S. Iijima, *Chem. Lett.* (1992) 1975;  
H. Tamaki, Z. J. Zhong, N. Matsumoto, S. Kida, M. Koikawa, Y. Aiihiwa,  
Y. Hashimoto and H. Ôkawa, *J. Am. Chem. Soc.* 114 (1992) 6974;  
S. Iijima, T. Katsura, H. Tamaki, M. Mitsumi, N. Matsumoto and H. Ôkawa,  
*Mol. Cryst. Liq. Cryst. Sci. Technol. A* 233 (1993) 263;  
S. Decurtins, S. W. Schmalle, H. R. Ostwald, A. Linden, J. Ensling, P. Gülich

- and A. Hauser, *Inorg. Chim. Acta* 216 (1994) 65;  
 C. Mathonière, S. G. Carling, Y. Dou and P. Day,  
*J. Chem. Soc. Chem. Commun.* (1994) 1554;  
 W. M. Reiff, J. Kreisz, L. Meda and R. U. Kirss,  
*Mol. Cryst. Liq. Cryst. Sci. Technol. A* 273 (1995) 181;  
 C. Mathonière, C. J. Nuttall, S. G. Carling and P. Day,  
*Inorg. Chem.* 35 (1996) 1201.
- [19] T. Kaneyoshi, Y. Nakamura and S. Shin,  
*J. Phys.: Condens. Matter* 10 (1998) 7025;  
 Y. Nakamura, *J. Phys.: Condens. Matter* 12 (2000) 4067;  
 Y. Nakamura, *Phys. Rev. B* 62 (2000) 11742;  
 Y. Nakamura, *Prog. Theor. Phys.* 138 (2000) 466;  
 G. M. Buendia and E. Machado, *J. Magn. Magn. Mater.* 272-276 (2004) 249.
- [20] L. L. Gonçalves, *Physica Scripta* 32 (1985) 248;  
 L. L. Gonçalves, *Physica Scripta* 33 (1986) 192;  
 J. W. Tucker, *J. Magn. Magn. Mater.* 95 (1999) 133.
- [21] R. B. Potts, *Phys. Rev.* 88 (1952) 352;  
 G. F. Newell, *Phys. Rev.* 79 (1950) 876;  
 R. M. F. Houtappel, *Physica* 16 (1950) 425;  
 H. N. V. Temperley, *Proc. Roy. Soc.* 203A (1950) 202;  
 R. J. Baxter and T. Choy, *Proc. Roy. Soc. London Ser. A* 423 (1989) 279;  
 J. H. Barry, T. Tanaka, M. Khatun and C. H. Múnera,  
*Phys. Rev. B* 44 (1991) 2595.
- [22] E. Balcar, S. W. Lovesey, *Theory of magnetic neutron and photon scattering*,  
 (Clarendon, Oxford, 1989).
- [23] T. Moriya, *Prog. Theor. Phys.* 16 (1956) 23.
- [24] M. Jaščur, S. Lacková, *J. Phys.: Condens. Matter* 12 (2000) L583.
- [25] M. Jaščur, J. Strečka, *Phys. Lett. A* 258 (1999) 47;  
 J. Strečka, M. Jaščur, *Acta Electrotechnica et Informatica* 2 (2002) 102  
 (cond-mat/0207519);  
 J. Strečka, H. Čenčariková, M. Jaščur,  
*Acta Electrotechnica et Informatica* 2 (2002) 107 (cond-mat/0207518);  
 H. Suzuki, M. Suzuki, *Int. J. Mod. Phys. B* 16 (2002) 3871;  
 J. Strečka, M. Jaščur, *J. Magn. Magn. Mater.* 260 (2003) 415;  
 Y. Fukumoto and A. Oguchi, *J. Magn. Magn. Mater.* 272-276 (2004) 910.

## Figure captions

Fig. 1 The segment of a mixed-spin honeycomb lattice. The lattice positions of the spin-1/2 (spin-3/2) atoms are schematically designated by the full (open) circles, the solid lines label the interactions between nearest-neighbouring atoms. The dashed lines represent the effective interaction between three outer spin-1/2 atoms, which arise after performing the mapping (9) at  $k$ th site.

- Fig. 2 a) The ground-state phase diagram in the  $E/J - D/J$  plane; b) The single-site sublattice magnetization  $|m_A|$  (dotted line) and  $m_B$  (dashed line), the total single-site magnetization  $|m|$  (solid line) and the quadrupolar momentum  $\eta$  (solid line) as a function of the biaxial anisotropy  $E/J$  at  $T = 0$  and  $D/J = 1.0$ .
- Fig. 3 The time variation of the dynamical autocorrelation function  $C_{auto}^{zz}$  at very low temperature ( $k_B T/J = 0.001$ ) close to the ground state: a) for  $D/J = 0.0$  and various  $E/J$ ; b) for  $E/J = 0.5$  and various  $D/J$ ; Time axis is scaled in  $\hbar/J$  units.
- Fig. 4 a) The dependence of critical temperature on the uniaxial anisotropy  $D/J$  for several values of biaxial anisotropies  $E/J$ ; b) The dependence of critical temperature on the biaxial anisotropy  $E/J$  for several values of uniaxial anisotropies  $D/J$ . Solid (broken) lines correspond to the critical temperatures of the OP<sub>1</sub> (OP<sub>2</sub>) phase. Open circles denote the critical temperatures for a such particular case, when both the ordered phases OP<sub>1</sub> and OP<sub>2</sub> coexist in the ground state (see the text).
- Fig. 5 The thermal dependences of the single-site magnetization for  $E/J = 0.5$  and: a)  $D/J = -2.0, 0.0, 0.5$  and  $0.75$ ; b)  $D/J = \sqrt{13}/4, 1.0$  and  $1.5$ . The dotted (dashed) lines stand for the sublattice magnetization  $|m_A|$  ( $m_B$ ), the solid lines for the total single-site magnetization  $|m|$ . Fig. 5b shows the temperature dependences of the sublattice magnetization  $|m_A|$  and  $m_B$  only, the insert shows the appropriate changes of the total magnetization  $|m|$ .
- Fig. 6 The time variation of the dynamical autocorrelation function  $C_{auto}^{zz}$  when  $E/J = 0.5$  is fixed and  $D/J$  is changed:  $D/J = -2.0$  (upper),  $0.0$  (central) and  $1.0$  (lower panel). The relevant time variations of  $C_{auto}^{zz}$  are displayed at three different temperatures, which are normalized with respect to their critical temperatures in order to get the ratio  $\tau = 0.75, 1.0$  and  $1.25$  in Fig. 6ab and respectively,  $\tau = 0.1, 0.25$  and  $1.0$  in Fig. 6c. Time axis is scaled in the  $\hbar/J$  unit.

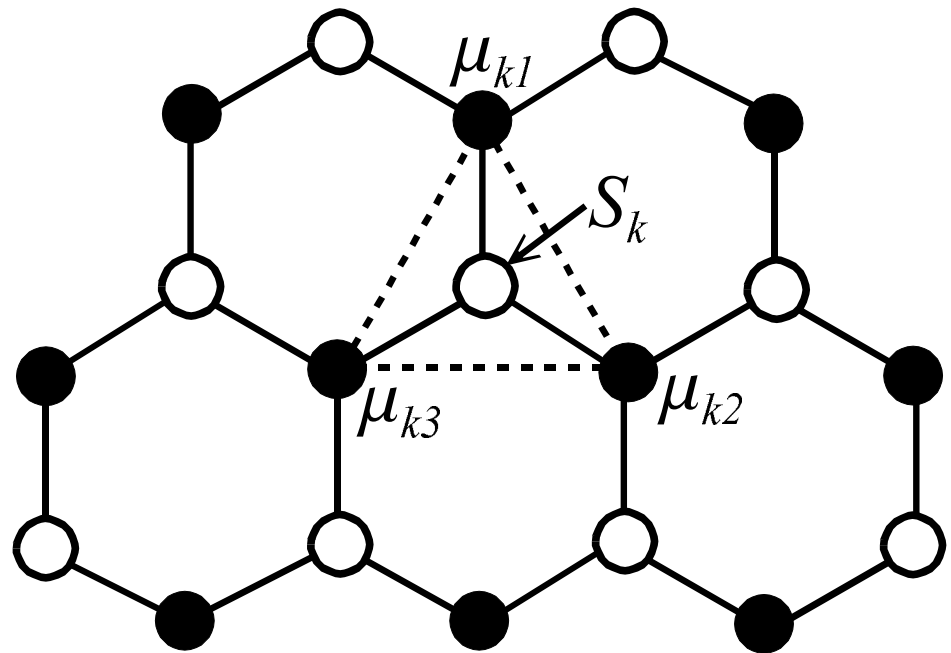


Fig. 1 Jascur et al.

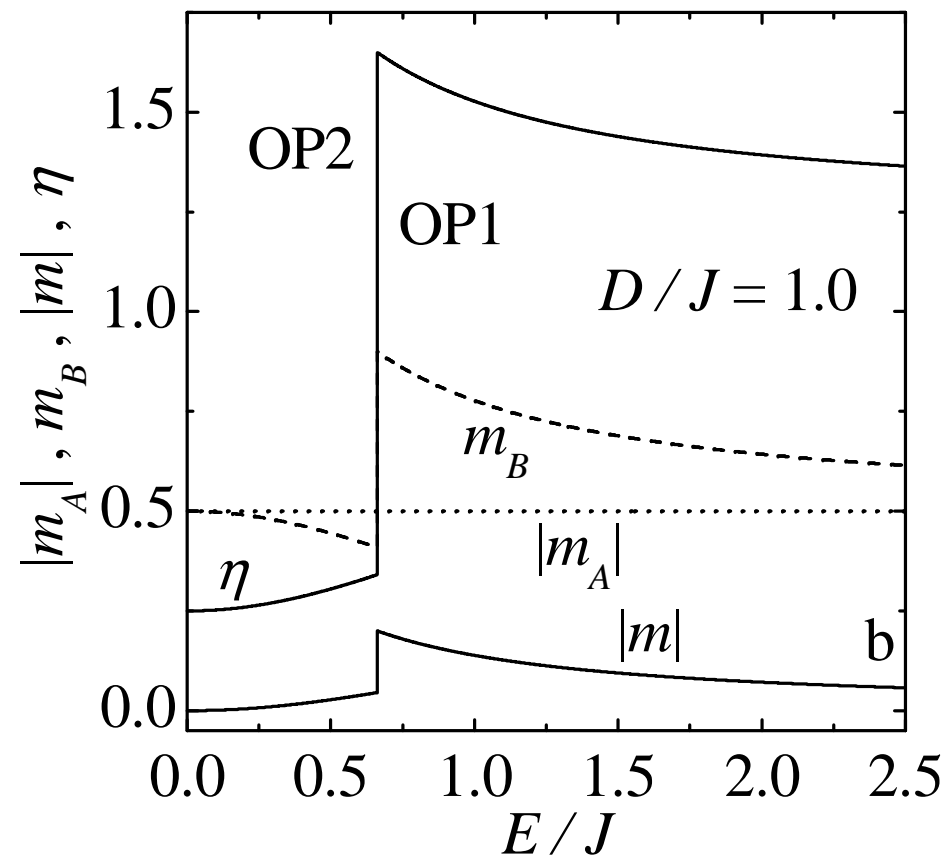
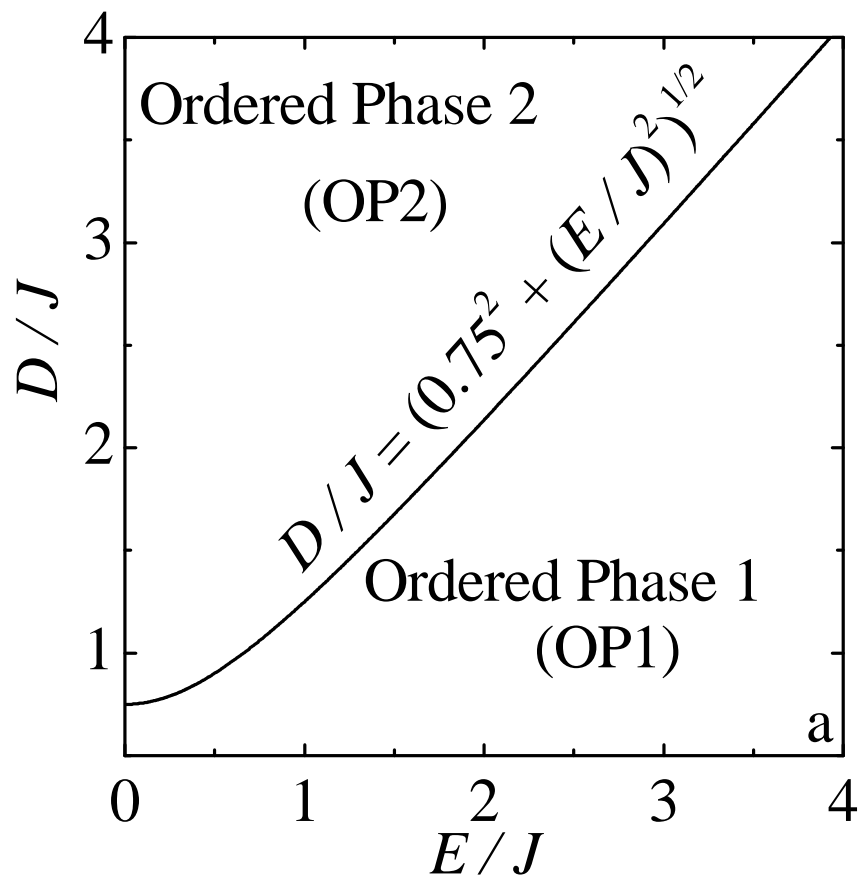


Fig. 2 Jascur et al.

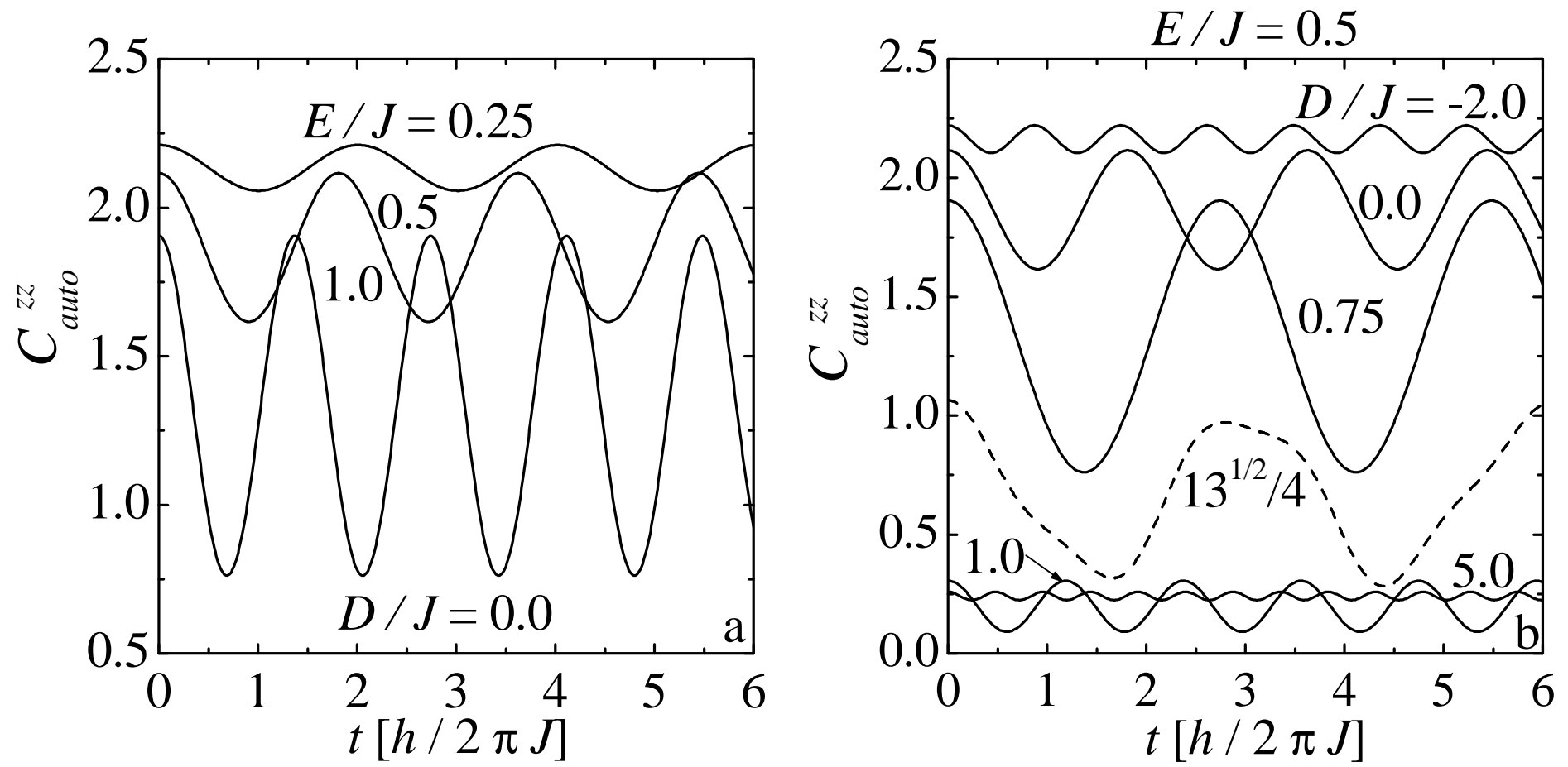


Fig. 3 Jascur et al.

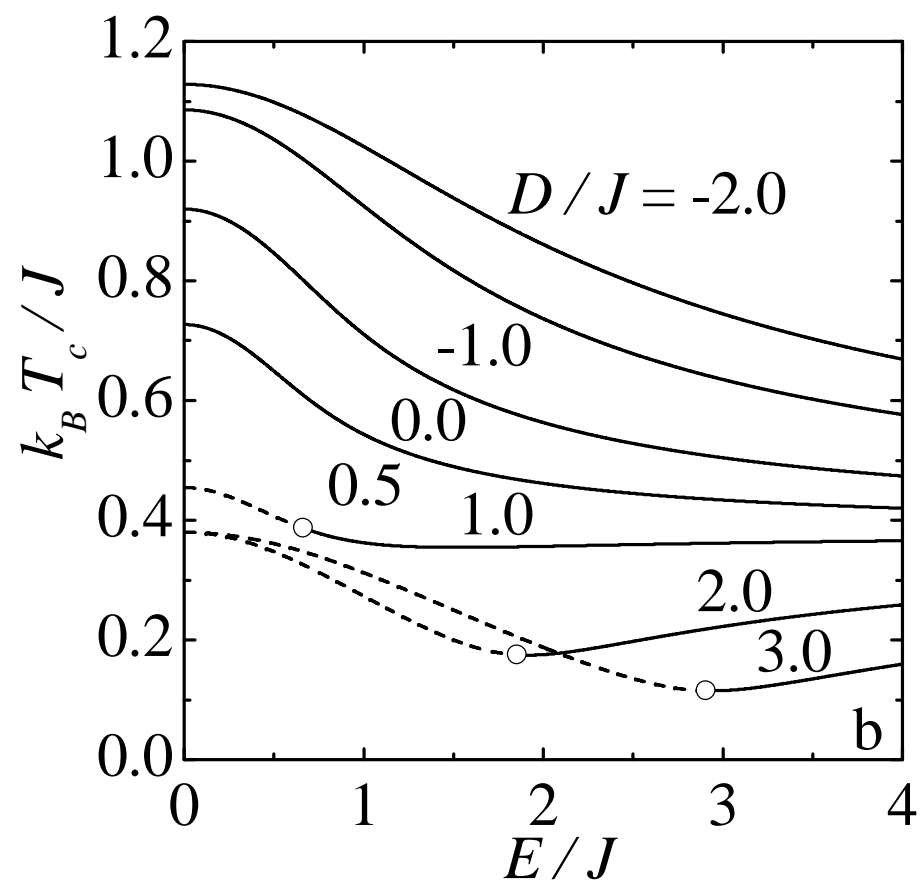
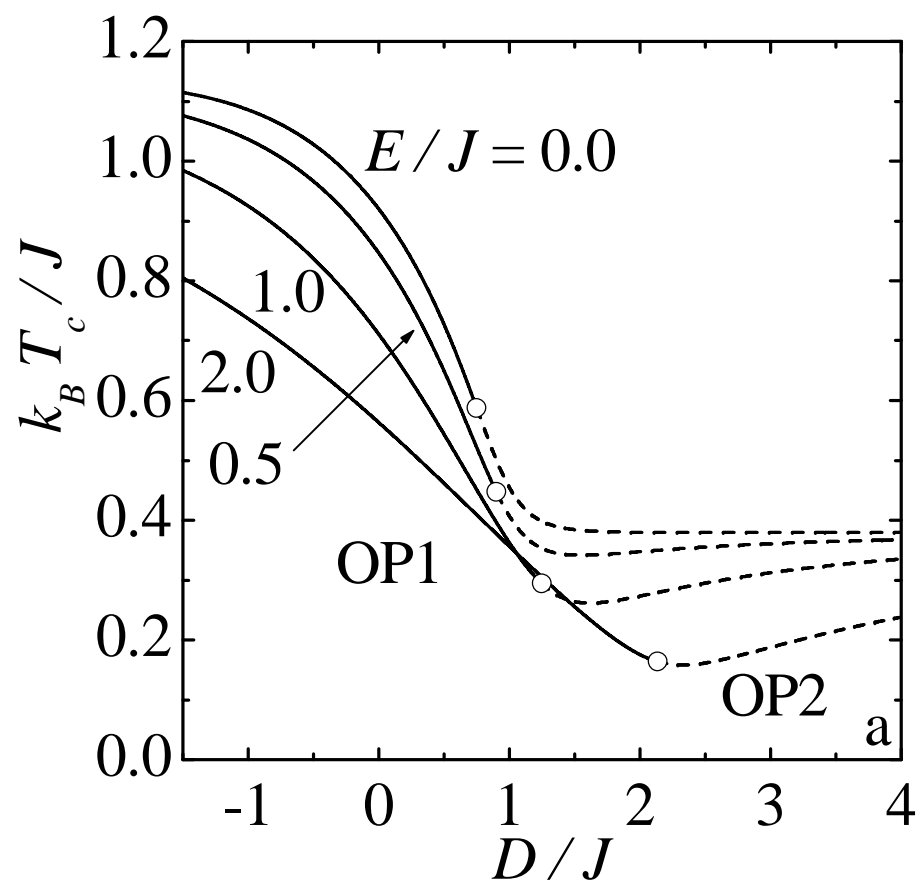


Fig. 4 Jascur et al.



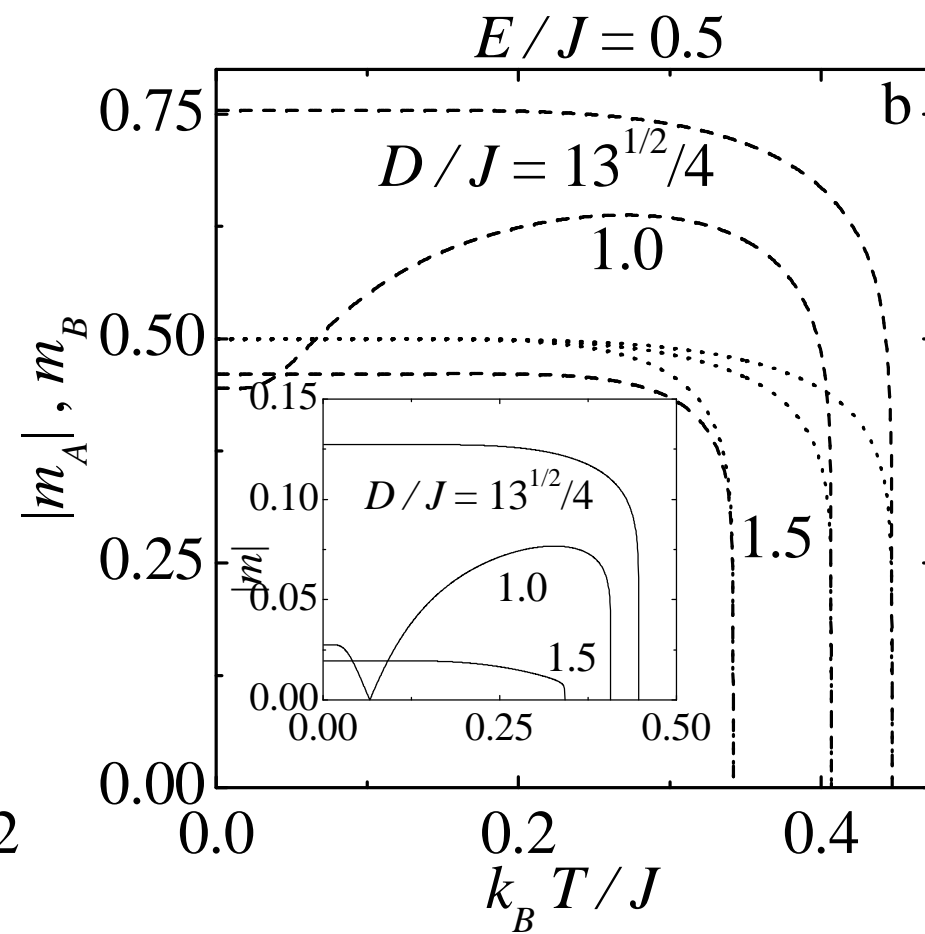
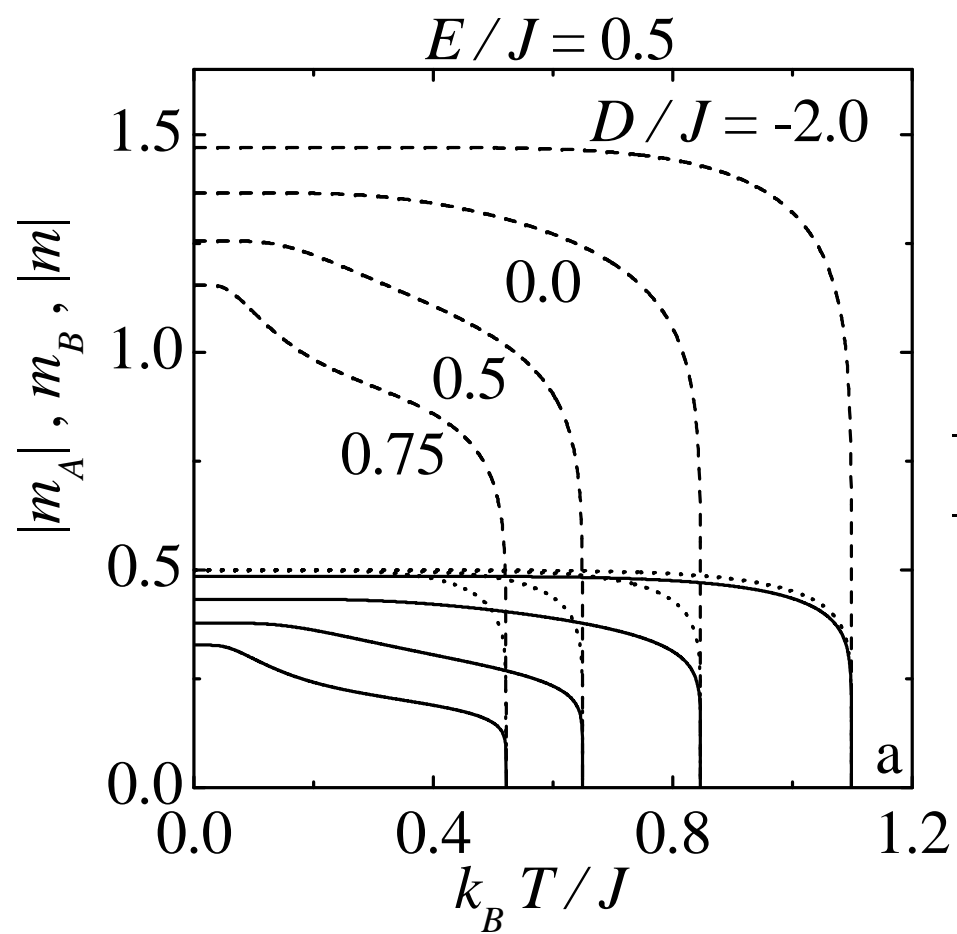


Fig. 5 Jascur et al.

